Supplementary Material for

Quantum State-to-State Study for $(H^-(D^-), HD)$ collisions on two Potential Energy Surfaces

Xiaohu He,[a] Wenliang Li,[b]* Huiyan Meng,[a] Chuanliang Li,[a]* Guqing Guo,[a] Xuanbing Qiu,[a] Jilin Wei[a]

[a] *Department of Physics, Taiyuan University of Science and Technology 030024, Taiyuan, China*

[b] *Department of physics, Xinjiang Institute of Engineering, 830091, Urumqi, Xinjiang, China*

*Corresponding author:

Wenliang Li (E-mail: wenliangli@vip.126.com)

Chuanliang Li (E-mail: clli@tyust.edu.cn)

Contents

1. Quantum dynamics calculation details

We repeat the title reactions here:

$H^- + HD \rightarrow H_2 + D^-$ (R1),

$H^- + HD \rightarrow HD + H^-$ (R2),

$D^- + HD \rightarrow HD + D^-$ (R3),

$D^- + HD \rightarrow D_2 + H^-$ (R4).

In the Supplementary Material, we will provide some calculation results which maybe helpful to understand the dynamics of the title reactions and the main text of the present work. In the text, E_c represents the collision energy, and θ represents the scattering angle.

It has been stated in the main text that the maximum value of the helicity quantum number (K_{max}) is set to 20. To prove that 20 is large enough, we here exhibit a set of dynamics results (including integral cross sections (ICSs) and differential cross sections (DCSs)) for $K_{max} = 12$ and $K_{max} = 20$ in Figures S1 – S8. In our calculations, the helicity quantum number K for each total angular momentum (J) is restrained by the equation $K \leq min(J, K_{max})$. It can be found that the results for $K_{max} = 12$ and $K_{max} = 20$ are fairly close to each other, indicating that the results demonstrated in the text are accurate enough. Figs. S1 and S2 show the total ICSs for the title reactions based on the AY[1] and PS[2] PESs, respectively. Figs. S3 – S8 exhibit several typical total and final state-resolved DCSs based on the two PESs.

Figure S1. Total integral cross sections for the R1, R2, R3 and R4 reactions based on the AY PES. The solid and dashed lines indicate the results for $\boldsymbol{K_{max} = 12}$ and 20, respectively.

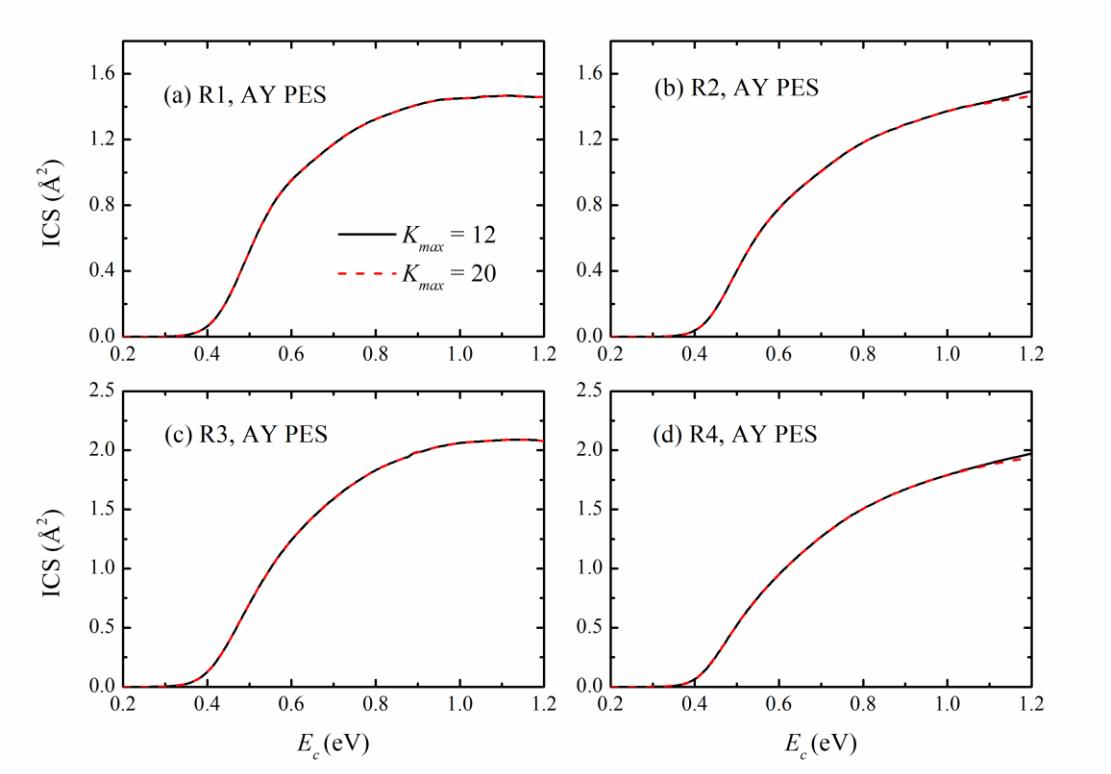

Figure S2. The same as Figure S1, but on the PS PES.

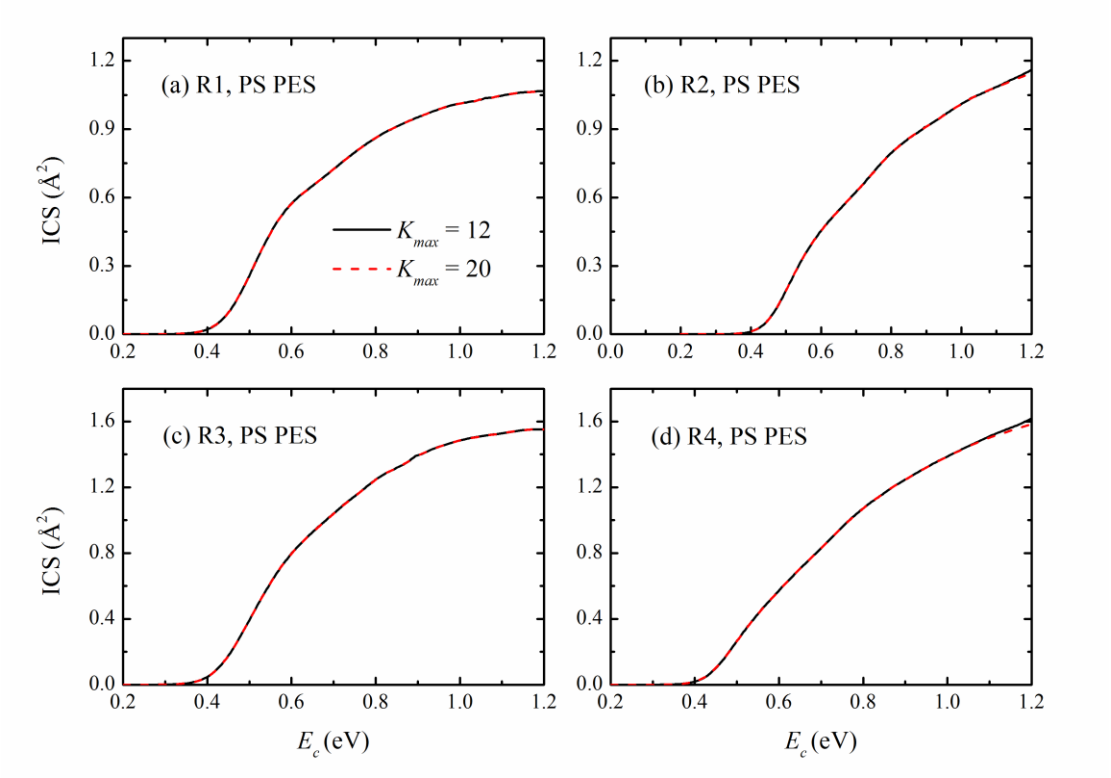

Figure S3. Total differential cross sections for the R1 and R2 reactions at the collision energies of 0.6 and 1.2 eV based on the AY PES. The solid and dashed lines indicate the results for $\boldsymbol{K_{max} = 12}$ and 20, respectively.

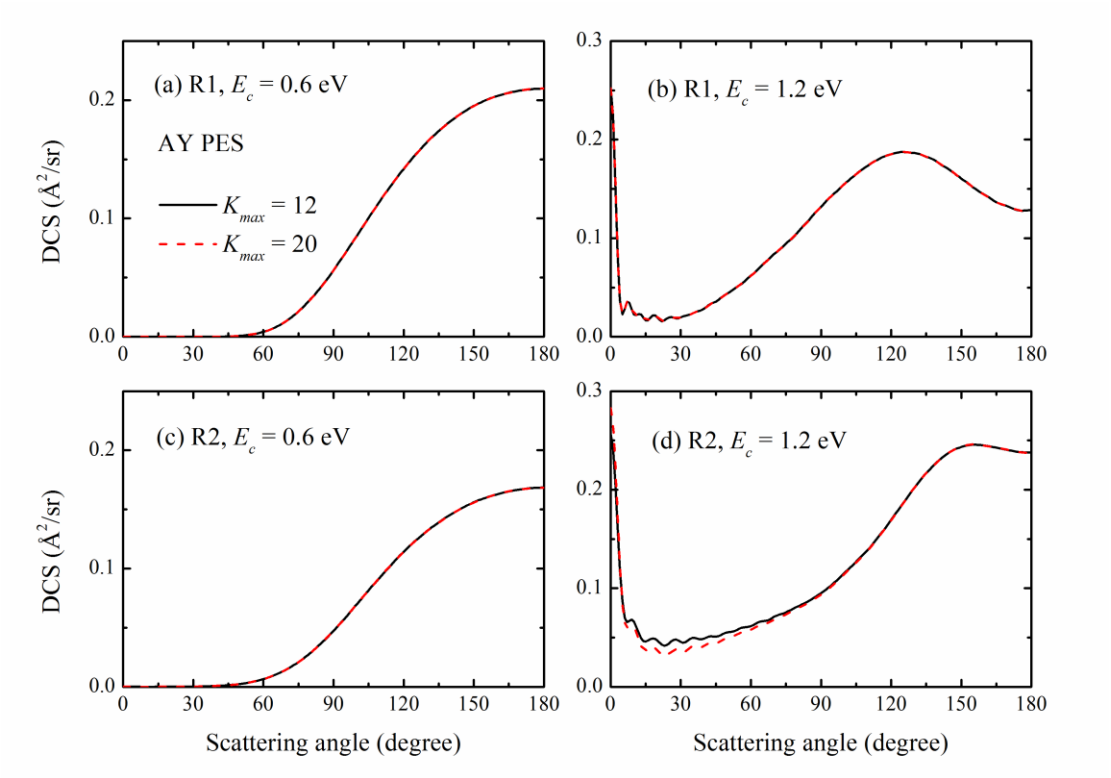

Figure S4. The same as Figure S3, but on the PS PES.

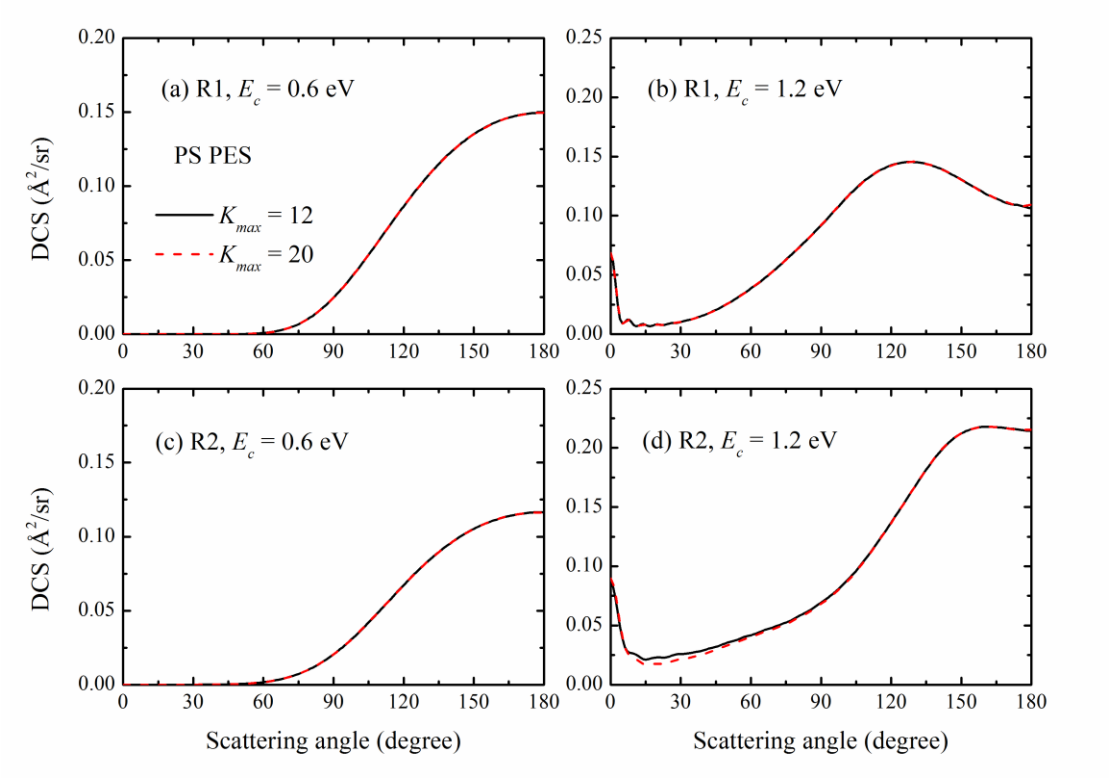

Figure S5. Product vibrational state-resolved ($\boldsymbol{v' = 0}$) differential cross sections for the R1 and R2 reactions at the collision energies of 0.6 and 1.2 eV based on the AY PES. The solid and dashed lines indicate the results for $\boldsymbol{K_{max} = 12}$ and 20, respectively.

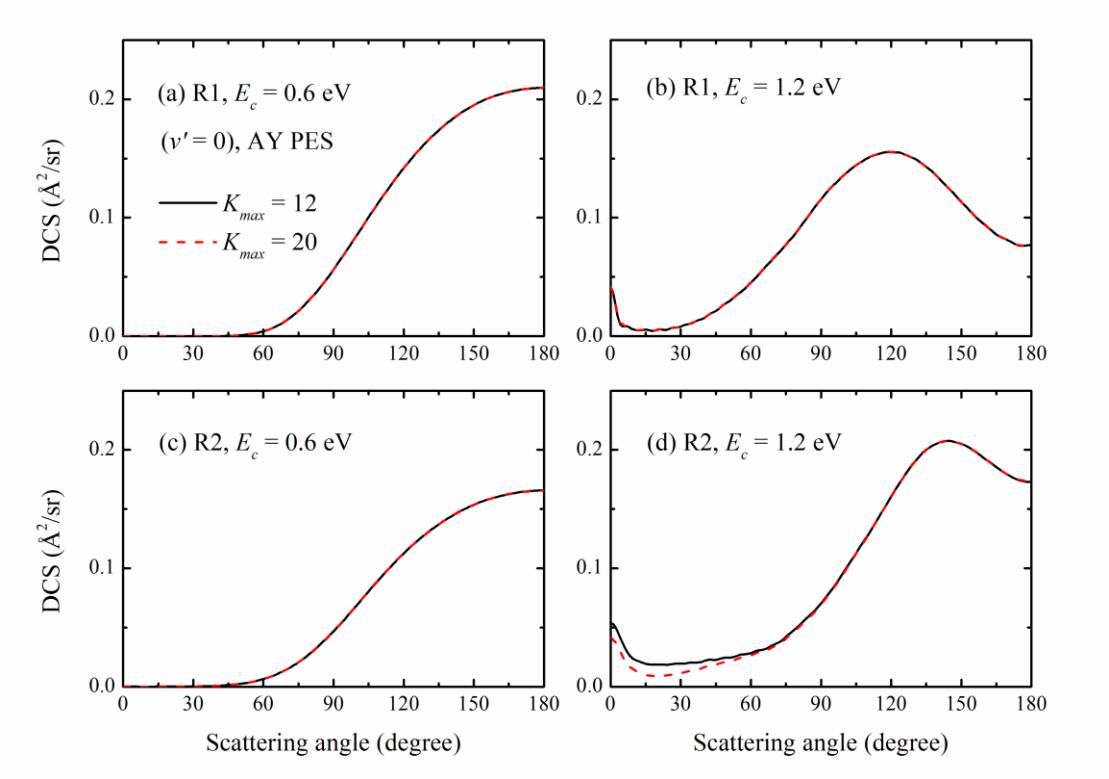

Figure S6. The same as Figure S5, but on the PS PES.

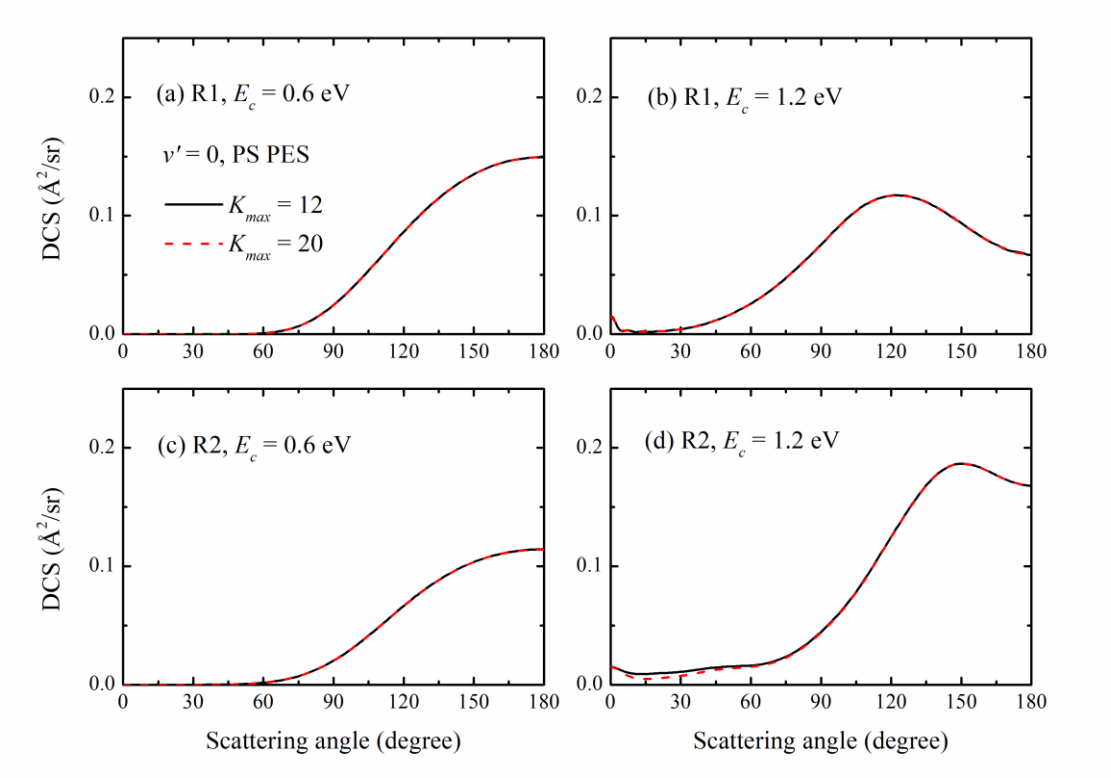

Figure S7. Product rovibrational state-resolved ($\boldsymbol{v' = 0, j' = 2}$) differential cross sections for the R1 and R2 reactions at the collision energies of 0.6 and 1.2 eV based on the AY PES. The solid and dashed lines indicate the results for $\boldsymbol{K_{max} = 12}$ and 20, respectively.

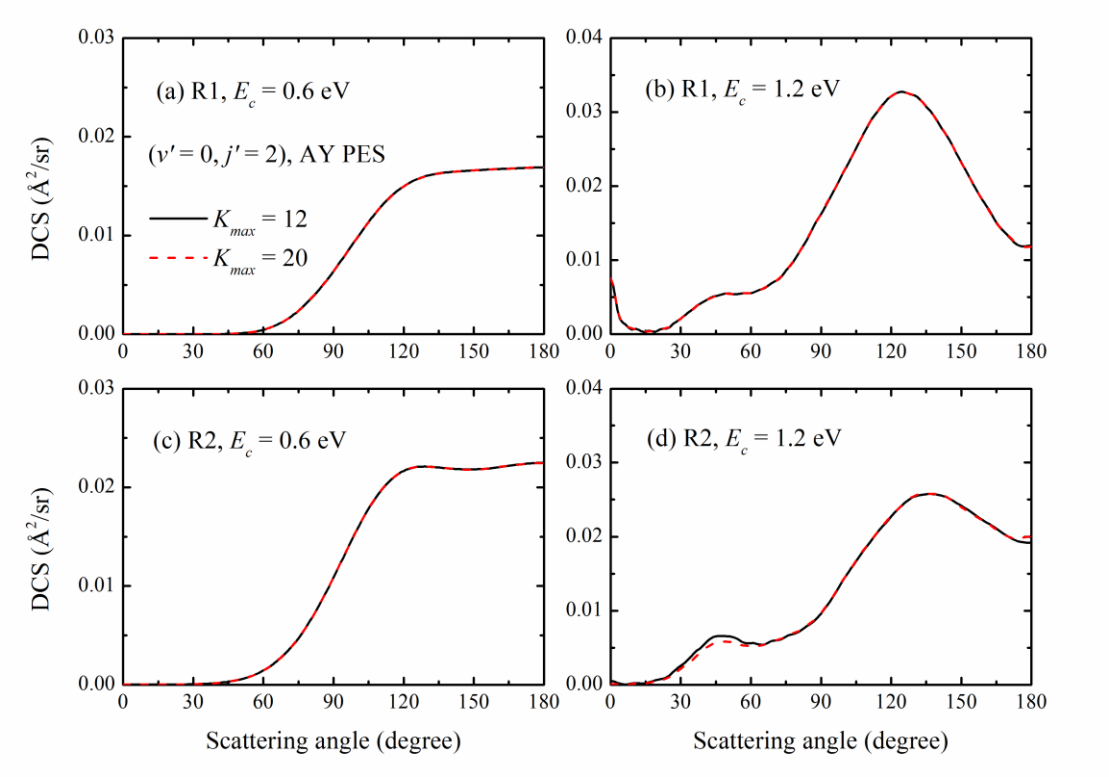

Figure S8. The same as Figure S7, but on the PS PES.

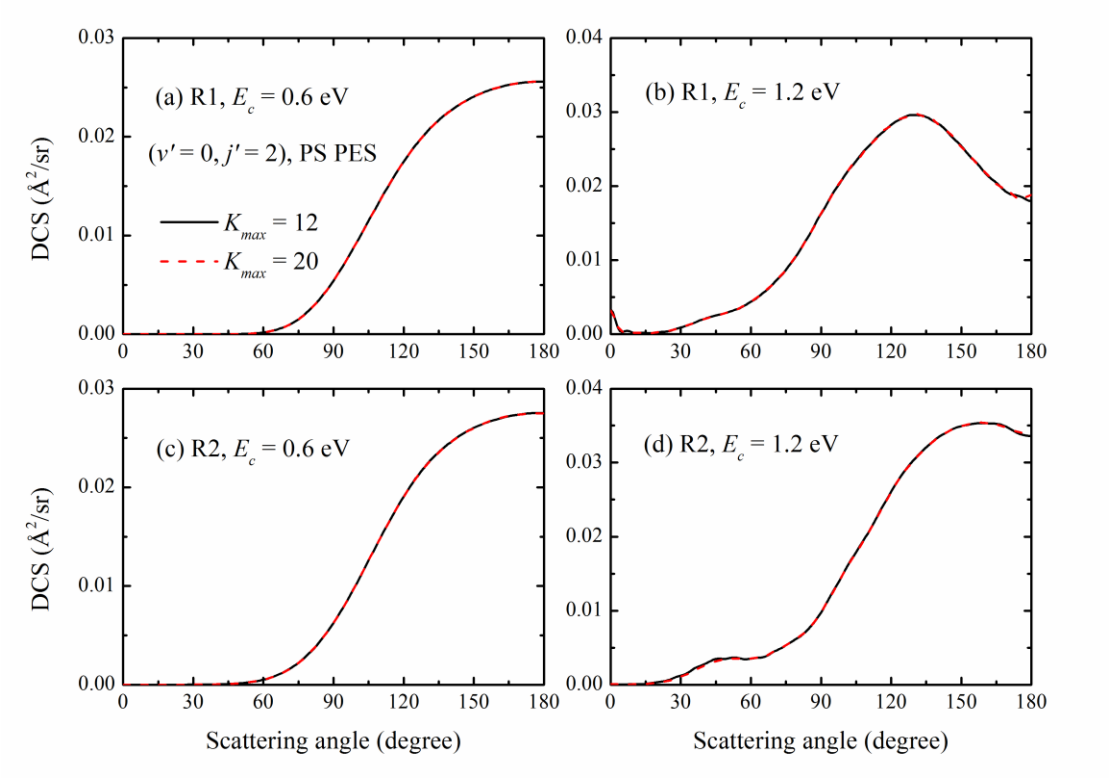

2. Total and final state-resolved differential cross sections for the $D^- + HD$ reaction

The DCSs for the R3 and R4 reactions are similar to the DCSs for R1 and R2, respectively. Fig. S9 shows the total DCSs for the R3 and R4 reactions at several collision energies based on the AY[1] and PS[2] PESs. Figs. S10 and S11 exhibit the product vibrational state-resolved ($v' = 0$ and 1) DCSs for the R3 and R4 reactions at the collision energies of 0.6 and 1.2 eV based on the AY and PS PESs. Figs. S12 and S13 exhibit the product rovibrational state-resolved DCSs for the R3 and R4 reactions at the collision energies of 0.6 and 1.2 eV based on the AY and PS PESs.

Figure S9. Total differential cross sections for the R3 and R4 reactions at the collision energies of 0.4, 0.6, 0.8, 1.0 and 1.2 eV based on the AY and PS PESs. The square, circle, up triangle, down triangle and diamond symbols are the results at the collision energies 1.2, 1.0, 0.8, 0.6 and 0.4 eV, respectively.

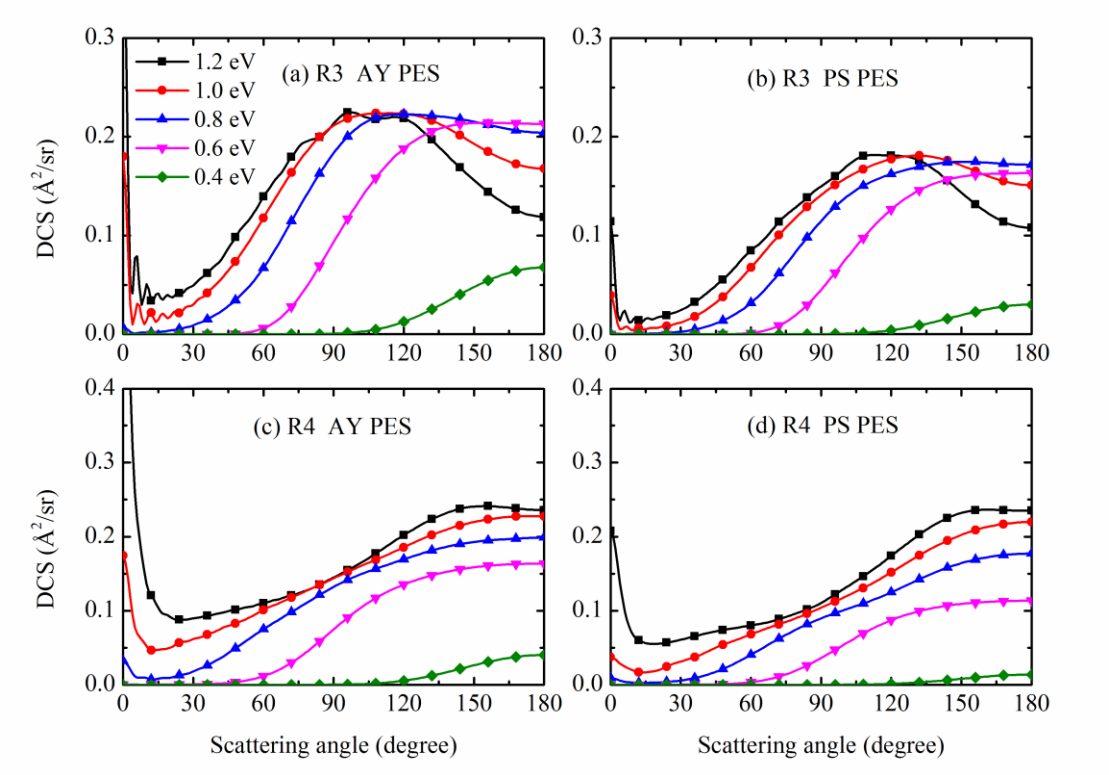

Figure S10. Product vibrational state-resolved ($v' = 0$) differential cross sections for the R3 and R4 reactions at the collision energies of 0.6 and 1.2 eV based on the AY and PS PESs. Panels a and b are the results at 0.6 eV, and panels c and d are the results at 1.2 eV. Left panels: results for R3. Right panels: results for R4. The solid and dashed lines are the results based on the AY and PS PESs, respectively.

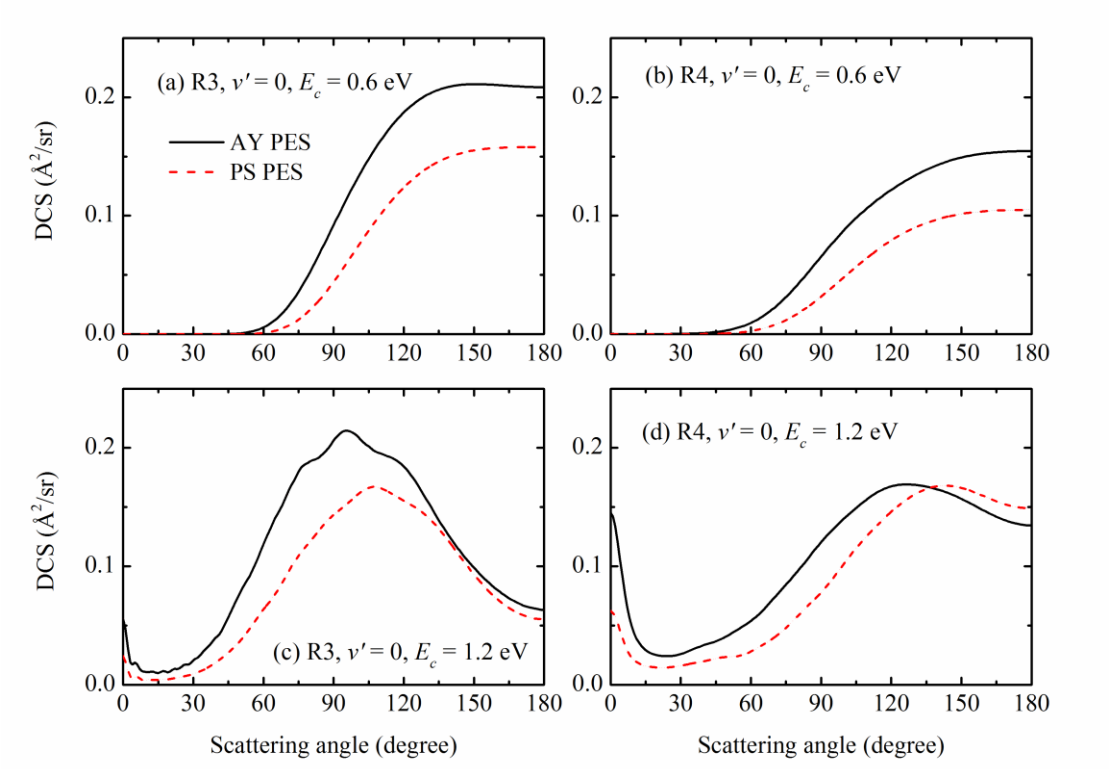

Figure S11. Product vibrational state-resolved ($v' = 1$) differential cross sections for the R3 and R4 reactions at the collision energy 1.2 eV based on the AY and PS PESs. Panel a: results for R3. Panel b: results for R4. The solid and dashed lines are the results based on the AY and PS PESs, respectively.

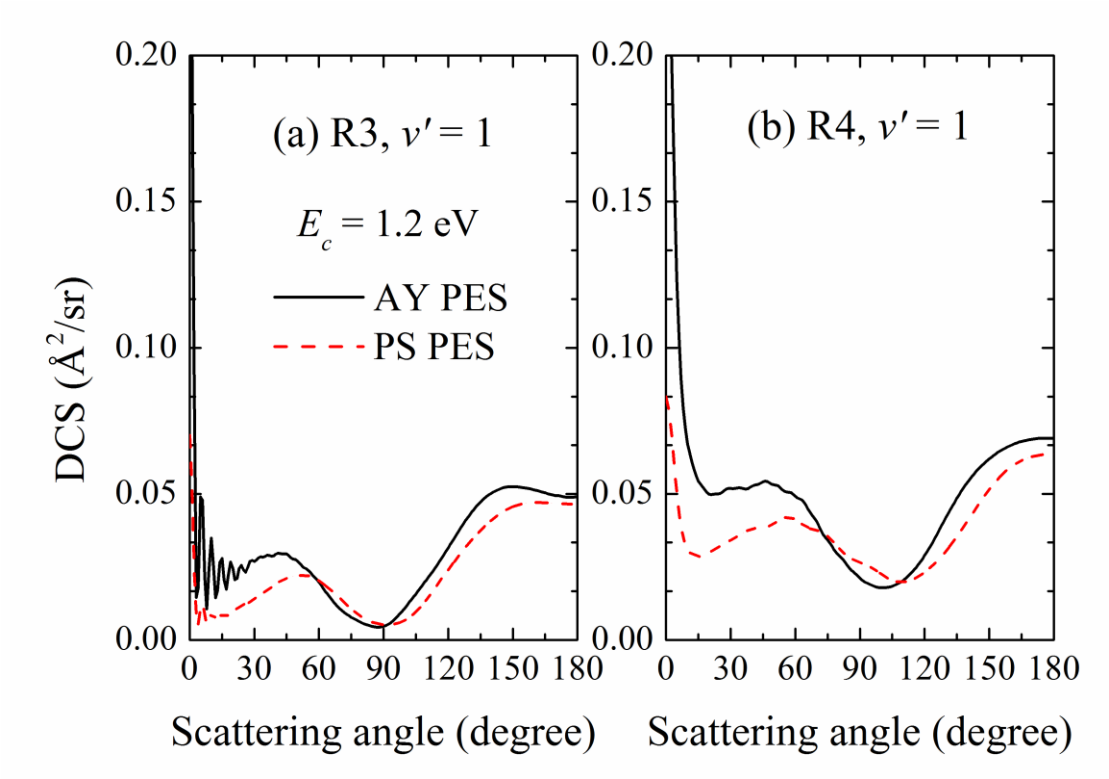

Figure S12. Product rovibrational state-resolved differential cross sections for the R3 reaction at the collision energies of 0.6 and 1.2 eV based on the AY and PS PESs. At 0.6 eV, only the $v' = 0$ results are depicted in the figure. At 1.2 eV, the $v' = 0$ and $v' = 1$ results are both included. Upper panels: differential cross sections based on the AY PES. Lower panels: differential cross sections based on the PS PES.

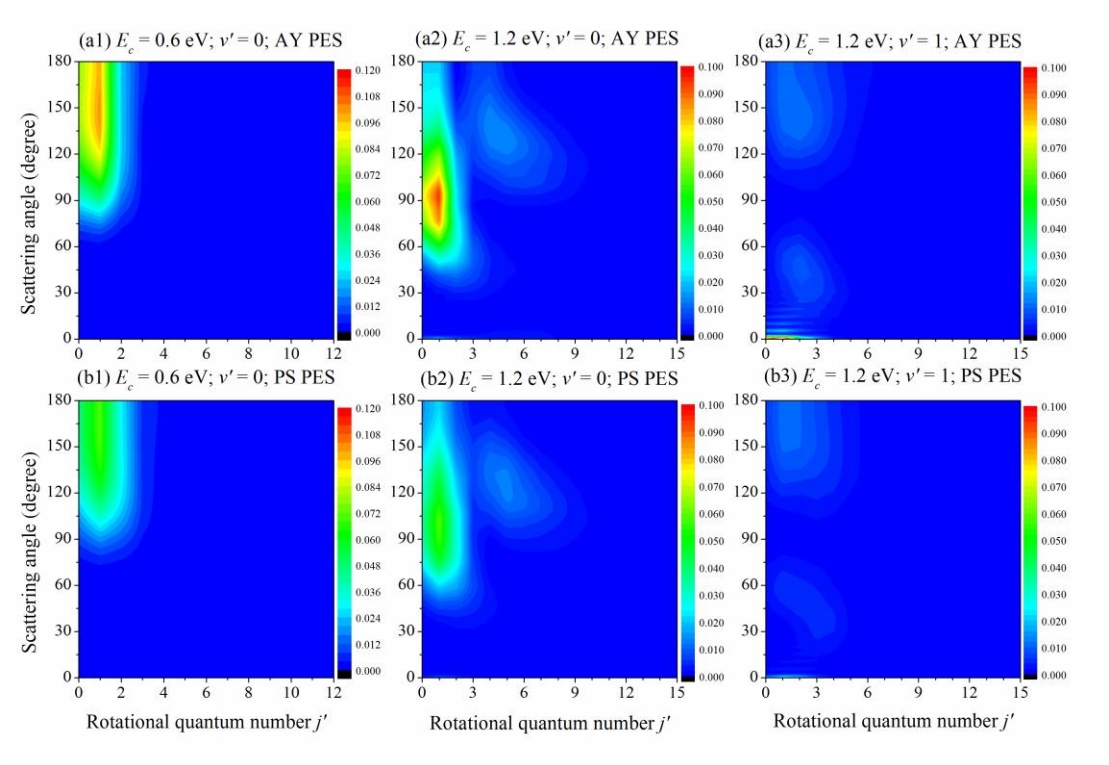

Figure S13. The same as figure S12 but for the R4 reaction.

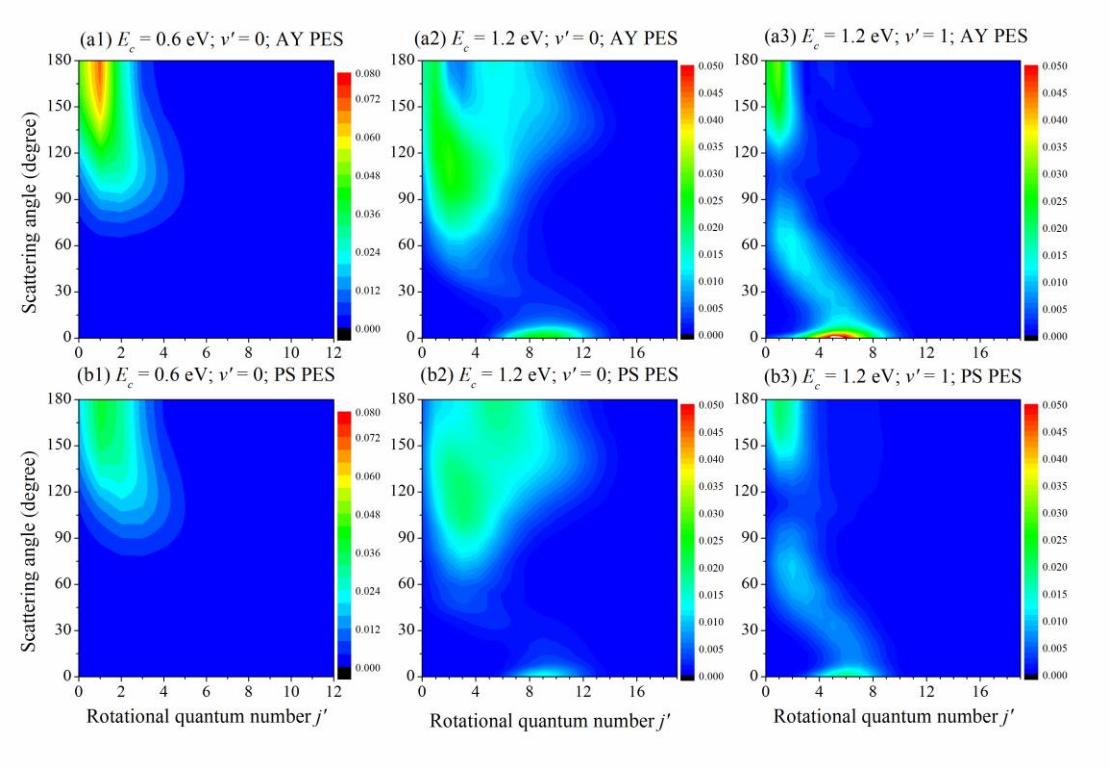

3. Typical differential cross sections and product rotational state distributions for the $H^- + HD$ reactionAY

Fig. S14 shows the DCSs calculated by the quasi-classical trajectory method[3-6] and the time-dependent wave-packet method[7-13] for the R1 and R2 reactions at 0.6 and 1.2 eV based on the AY PES. The two sets of differential cross sections are quite similar to each other. Fig. S15 exhibit the product vibrational state-resolved ($v' = 0$) DCSs for the R1 and R2 reactions at the collision energy 1.2 eV based on the AY PES. Fig. S16 shows the product rotational state distribution of the $v' = 0$ product for the R1 and R2 reactions in the scattering angle range 0 – 10 º. The dynamics results shown in Figs. S15 and S16 are calculated by the QCT method.[3-6] The fitting procedure of the DCSs and the calculation method of collision time are introduced elsewhere (see Ref. 6 and the references therein). Panels a1 and a2 of Fig. S15 indicate that the convergence of backward scattering is earlier than that of forward scattering. Moreover, panels b1 and b2 of Fog. S15 indicate that the forward scattering for R1 appears later than that of R2, which could be considered as a time-delayed phenomenon. Fig. S16 shows that the forward scattered product of R1 has a relatively colder final rotational state distribution than that of R2, which could also be a possible evidence to distinguish the time-delayed mechanism and the stripping mechanism.

FigureS14. Differential cross sections for the R1 and R2 reactions at the collision energies of 0.6 and 1.2 eV based on the AY PES. The solid and dashed lines are the results calculated by the quasi-classical trajectory method and the time-dependent wave-packet method, respectively. Panels a and b are the results at 0.6 eV, and panels c and d are the results at 1.2 eV. Left panels: results for R1. Right panels: results for R2.

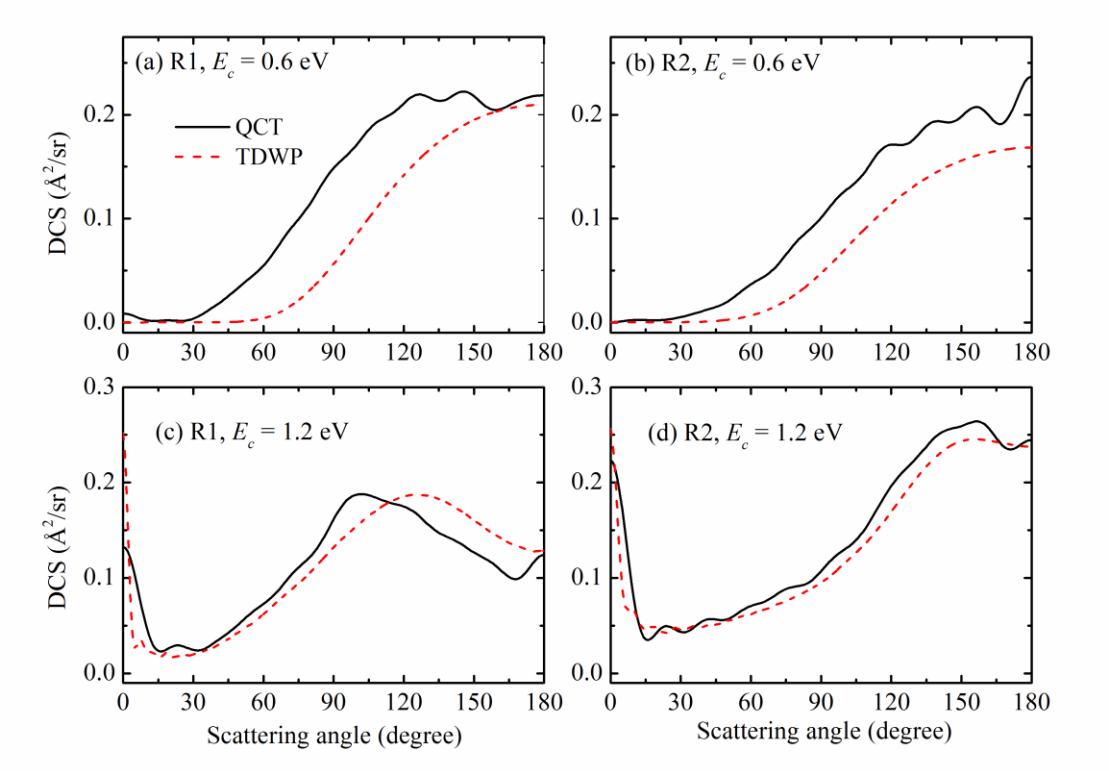

Figure S15. Product vibrational state-resolved ($\boldsymbol{v' = 0}$) differential cross sections for the R1 and R2 reactions at the collision energy 1.2 eV based on the AY PES. These results are calculated by the quasi-classical trajectory method. Left panels: differential cross sections at the collision time range of 23 – 100 fs for the R1 reaction. Right panels: the same as left panels but for the R2 reaction. Panels a1 and a2: results include the whole scattering angle range 0 – 180 º. Panels b1 and b2: results that in the scattering angle range 0 – 20 º.

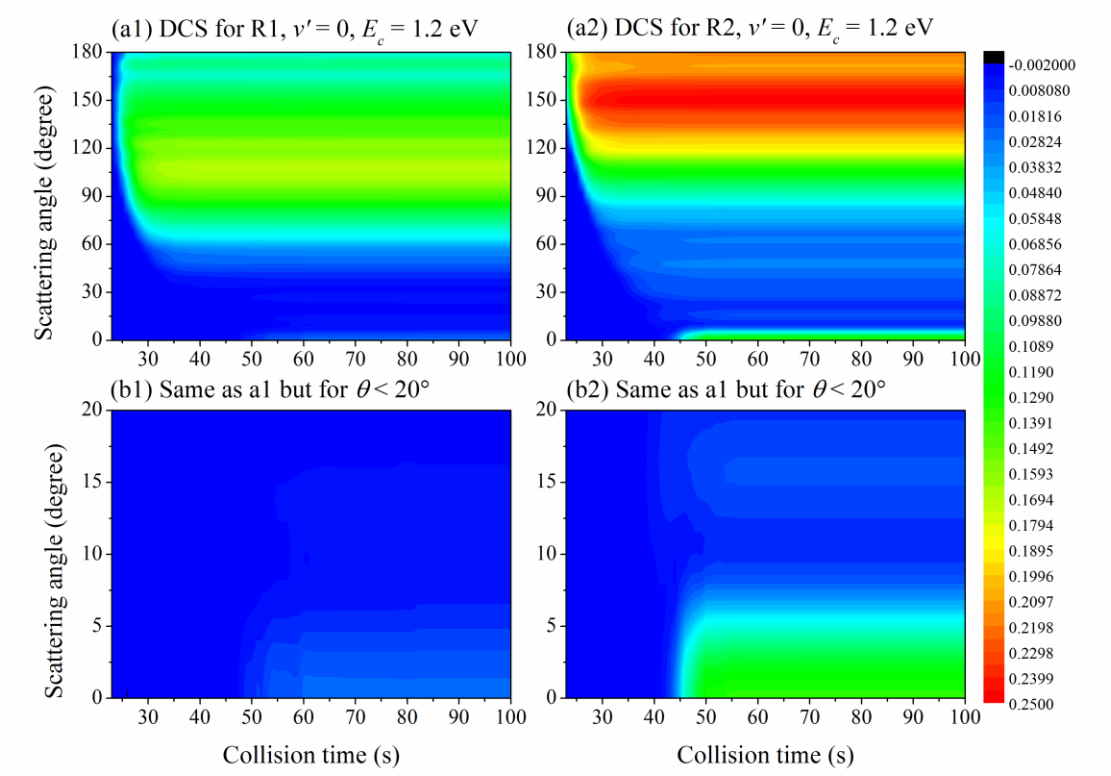

Figure S16. Product rotational state distribution of the $\boldsymbol{v' = 0}$ product for the R1 and R2 reactions in the scattering angle range 0 – 10 º. The square and circle symbols are the results for R1 and R2, respectively.

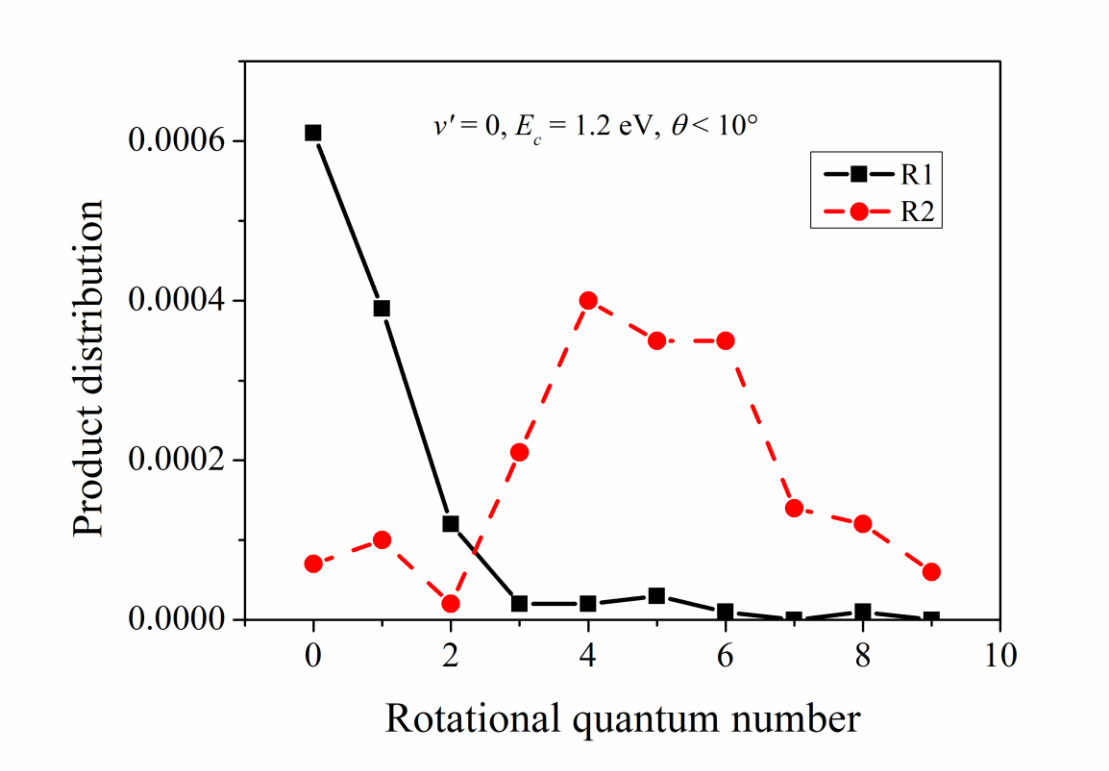

References

1 M. Ayouz, O. Dulieu, R. Guérout, J. Robert and V. Kokoouline, *J. Chem. Phys.*, 2010, **132**, 194309.

2 A. N. Panda and N. Sathyamurthy, *J. Chem. Phys.*, 2004, **121**, 9343.

3 D. G. Truhlar and J. T. Muckerman, in: R. B. Bernstein (Ed.), Atom - Molecule Collision Theory: A Guide for the Experimentalists, Plenum Press, New York, 1979.

4 F. J. Aoiz, V. J. Herrero and V. S. Rabanos, *J. Chem. Phys.*, 1992, **97**, 7423.

5 Z. X. Duan, W. L. Li, W. W. Xu and S. J. Lv, *J. Chem. Phys.*, 2013, **139**, 094307.

6 X. He, V. W.-K. Chao (Wu), K. Han, C. Hao and Y. Zhang, *Comput. Theor. Chem.*, 2015, **1056**, 1.

7 P. Y. Zhang and K. L. Han, *J. Phys. Chem. A*, 2013, **117**, 8512.

8 P. Y. Zhang and K. L. Han, *J. Phys. Chem. A*, 2014, **118**, 8929.

9 P. Y. Zhang and K. L. Han, *Int. J. Quan. Chem.*, 2015, **115**, 738.

10 X. H. He, H. Wu, P. Y. Zhang and Y. Zhang, *J. Phys. Chem. A*, 2015, **119**, 8912.

11 X. H. He, S. J. Lv, T. Hayat and K. L. Han, *J. Phys. Chem. A*, 2016, **120**, 2459.

12 T. S. Chu, Y. Zhang and K. L. Han, *Int. Rev. Phys. Chem.*, 2006, **25**, 201.

13 Z. G. Sun, H. Guo and D. H. Zhang, *J. Chem. Phys.*, 2010, **132**, 084112.